International Journal of Fluid Power 13 (2012) No. 3 pp. 25-37

ADAPTIVE PNEUMATIC CONTROL WITH SPOOL DEADBAND COMPENSATION

Eric Wolbrecht and Lucas Wells

University of Idaho, Department of Mechanical Engineering, PO Box 440902, Moscow, ID 83844-0902
ewolbrec@uidaho.edu, lucaswells@vandals.uidaho.edu

Abstract

This paper presents a novel approach to both adaptive deadband compensation and complete adaptive pneumatic control for a pneumatic servo control system driven by spool-type pneumatic proportional directional control valves. The controller is capable of either combined position and compliance control or combined force and compliance control. The novel adaptive approach includes control valve deadband compensation and adaptation for load variations and system mechanical properties. The control valve deadband compensation uses adjustable deadband lengths that are adapted to improve force tracking performance. The learned deadband model is then used in the complete adaptive controller, which includes adaptation for system mass, damping, and external load. The complete controller demonstrated accurate and stable force and position control for the tracking of sine, square, and sawtooth waveforms from 1 to 5 Hz.

Keywords: adaptive control, pneumatics, proportional control valve, deadband compensation

1 Introduction

In a typical pneumatic servo system a spool-type pneumatic proportional directional control valve is used to control the flow of air into and out of a pneumatic cylinder. From the standpoint of controllability, the ideal spool valve would produce a mass flow that is linear to the valve's electrical set point. Real proportional spool valves, however, have several nonlinearities that must be accounted for in the pneumatic servo system controller. First, the spool valve controls the orifice size only, but flow through the valve is a function of system pressures on both sides of the valve. Second, because spool-type valves do not contain seals, air will leak through the valve proportional to the pressure differential across the valve.

The final and potentially most difficult nonlinearity in a spool-type pneumatic valve is the deadband zone (region of low flow) around the midpoint of the valve. The deadband is caused by spool overlap which is intended to reduce air leakage at the midpoint, or zero-flow point, of the spool valve. In some cases, a manufacturer may offer the option of reducing spool overlap to reduce the deadband zone. Because this increases valve leakage, this option is not desirable for many applications.

This manuscript was received on 20 June 2011 and was accepted after revision for publication on 15 June 2012

One way to approach the problem of the spool valve nonlinearities is to model the flow dynamics and the orifice size as a function of spool setpoint (Richer, 2000; Shen, 2007; Xiang, 2004). Such model based methods approximate the actual flow conditions present but do not account for time-varying effects of valve wear and supply pressure change. Because these theoretical models are sometimes difficult to make accurate, an alternative approach is sometimes used, where flow characteristics of the spool valve are experimentally identified (Bobrow, 1998; Wolbrecht, 2009). Unfortunately, the experimental process may require a long data collection process and difficult curve fitting, and must be repeated when a different spool valve is used.

Because the deadband nonlinearity can be particularly disruptive to control, it is often directly addressed, through modeling (Valdiero, 2008) and/or identification (Valdiero, 2005). As an alternative, the deadband problem has been addressed through fuzzy-sliding, sliding-mode, or other control approaches (Bone, 2007; Knohl, 2000; Renn, 2002; Smaoui, 2008). The deadband problem has also been considered for more general nonlinear control systems (Recker, 1991; Selmic, 2000; Tao, 1995). In other applications, adaptation has been used in an attempt to improve controller perform-

ance (Bobrow, 1996; Gross, 1998; Kosaki, 1997).

This paper presents a novel approach to adaptive deadband compensation as part of a complete adaptive pneumatic controller. The main advantage of this approach is the ability to learn a deadband model without the need for making mass flow measurements. The deadband compensation is based on an adaptive model of the flow through the deadband region including deadband limit positions (both positive and negative) and mass flow leakage. Furthermore, the model is invertible, so that the control voltage required to produce the desired mass flow may be solved for explicitly. During application, the deadband model is learned during an initial force tracking calibration period, and is then fixed during normal pneumatic servo system operation, including force and position control. The deadband model may be relearned if a new valve is introduced or extensive wear is apparent.

The deadband compensation also includes an adaptive leakage term that corrects for air leakage across the spool valve (air leakage is airflow that exists due to a lack of a tight seal at the valve center position). This can be a significant percentage of mass flow and is typically un-accounted for in pneumatic control system, or is set to some constant value. The actual leakage is dependent on the supply, chamber, and atmospheric pressures, and is adaptively changed online during force and position control.

In addition to deadband compensation, the approach presented here also includes an adaptive 2nd order system model to compensate for changing external loads, variable friction, and unknown or unmodeled system dynamics. This gives the adaptive pneumatic controller the ability to provide accurate position tracking during changing environmental conditions while remaining compliant.

In the following sections, the adaptive pneumatic controller is developed and experimental tests are presented demonstrating the ability of the controller to provide accurate force and position tracking. The first experimental results demonstrate the ability of the adaptive deadband model to learn and compensate for the deadband region nonlinearities in the pneumatic proportional control valve. Additional experiments demonstrate the effectiveness of the control to provide accurate force and position tracking.

2 Adaptive Pneumatic Position and Force Control

Lyapunov based control is chosen to allow for a mathematical proof of stability for control of the nonlinear pneumatic system. This method of control also allows for combined position and force control, as well as parameter adaptation (Spong, 1989). An adaptive element is incorporated that lets the controller adapt to changing environmental conditions (such as gravity, viscous friction, and mass), and another adaptation learns an approximation of the nonlinear effects of the spool-type valves including both valve deadband and air leakage. In theory, this should allow the controller to fit many pneumatic servo systems with many combinations of servovalves, actuators, and loads.

First, the linear pneumatic actuation system is described and then the Lyapunov stable combined position and force control is developed. Finally, the controller gain tuning procedure is presented.

2.1 Pneumatic Cylinder Net Force Control

A double-acting pneumatic cylinder is a linear actuator that has two separate air chambers that may be individually pressurized. The force of the base side, f_1, and rod side, f_2, of the cylinder create a combined total force, F, on the mobile part so that:

$$F = f_1 - f_2 - f_{atm} \tag{1}$$

where f_{atm} is the external force on the rod due to atmospheric pressure.

The combined total force can be controlled with a single 5/2 valve. However, in order to control compliance (as well as total force), a proportional valve is needed for each chamber. The pneumatic cylinder and proportional valve system is shown in Fig. 1 below. The variables in Fig. 1 are detailed in the paragraphs following.

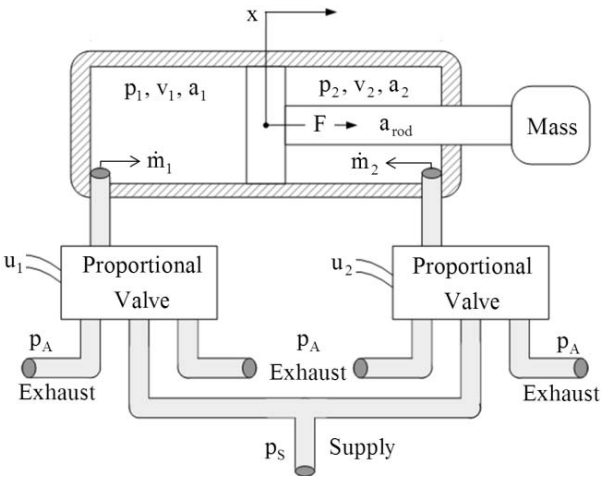

Fig. 1: *Pneumatic servo positioning system*

The pneumatic servo system consists of the stroke position, x, base side chamber pressure, p_1, and rod side chamber pressure p_2 (all notation will use subscripts 1 and 2 for the base and rod sides, respectively). The valve control signals, $u_{1,2}$, control the mass flow into and out of the cylinder chambers.

By assuming an adiabatic process and treating air as an ideal gas, the pressure dynamics in the base and rod side chambers of the cylinder can be approximated in terms of forces f_1 and f_2, respectively, as (McCloy, 1980):

$$\dot{f}_{1,2} = \gamma RT \frac{a_{1,2}}{v_{1,2}} \dot{m}_{1,2} - \gamma \frac{\dot{v}_{1,2}}{v_{1,2}} f_{1,2} \tag{2}$$

where γ is the ratio of specific heats of air ($\gamma = C_p / C_v = 1.4$), R is the universal gas constant, T is the temperature which is assumed constant, $a_{1,2}$ are the piston areas, $v_{1,2}$ are the chamber volumes, and $\dot{m}_{1,2}$ are the mass flow rates into the chambers.

2.2 Lyapunov Based Adaptive Pneumatic Controller

A Lyapunov based control approach provides a reliable template for proof of stability for a controller using the direct method (Spong, 1989). In addition, this approach allows the adaptation parameters to fit changing system parameters while the system is online. The controller developed is adapted from a previous pneumatic controller (Wolbrecht, 2009) that is based on passivity-based motion control. The implemented hybrid position and force control measured a flow map to translate the pressure and desired mass flow rate into a proportional valve control signal. The earlier work of Bobrow (1998) used empirical proportional valve flow modelling as well as incorporating the thermodynamic properties of compressed air. The controller presented here uses adaptation instead of complex flow modelling to estimate mass airflow rate through the proportional valve deadband region. This reduces the need for experimental mass flow measurements and eliminates the need of an expensive mass flow sensor.

A block diagram of the pneumatic servo positioning system is shown in Fig. 2. The plant consists of a double acting pneumatic cylinder and a proportional valve for each cylinder chamber. The measured plant outputs are base and rod pressures, p_1 and p_2, and the rod stroke position,. x The desired net force on the rod, F^{d}, is found using position and velocity errors and the adapted model. The desired base and rod chamber forces, f_1^d and f_2^d, are separated and smoothed from the net desired force. The desired mass flow rates, $\dot{m}_1^d$ and $\dot{m}_2^d$, are fed through the adaptive valve compensator to create the proportional valve control signals, u_1 and u_2

In the sections that follow, the system variables and model are defined. The adaptive second order mechanical system is then extracted from the model. Next, the valve model for the nonlinear flow through the pneumatic proportional valves is developed. Then, a Lyapunov candidate function is used to create control equations. Finally, the procedure for controller gain tuning is explained.

2.3 System Dynamics Model

The adaptive position control uses a sliding surface, s, and a reference trajectory, w, along with a positive gain, Λ, to calculate the desired force as described by Slotine (1987) and summarized by Spong (1989):

$$s = \dot{\tilde{x}} + \Lambda\tilde{x} = \left(\dot{x} - \dot{x}_{\mathrm{d}}\right) + \Lambda\left(x - x_{\mathrm{d}}\right) \tag{3}$$

$$w = \dot{x}^{\mathrm{d}} - \Lambda\tilde{x} = \dot{x}^{\mathrm{d}} - \Lambda\left(x - x^{\mathrm{d}}\right). \tag{4}$$

With these definitions, velocity and acceleration are directly related to the sliding surface and reference trajectory for use in the system model by $\ddot{x} = \dot{s} + \dot{w}$ and $\dot{x} = s + w$.

Bobrow (1989) demonstrated that a second order linear system converges to stable adapted states when adapting a model of the unknown dynamics for a pneumatic system better than higher order models. The second order model for our system is then:

$$m\ddot{x} + c\dot{x} + kx + \eta = f_1 - f_2 \tag{5}$$

where m is mass, c is viscous damping, k is the external load stiffness, η is an external weight force that includes the external force on the rod due to atmospheric pressure, and f_1 and f_2 are the base and rod forces on the system from the pneumatic chambers, respectively. The substitution of Eq. 3 and 4 into the system model Eq. 5 results in:

$$m\dot{s} + mw + c\dot{x} + kx + \eta = f_1 - f_2 \tag{6}$$

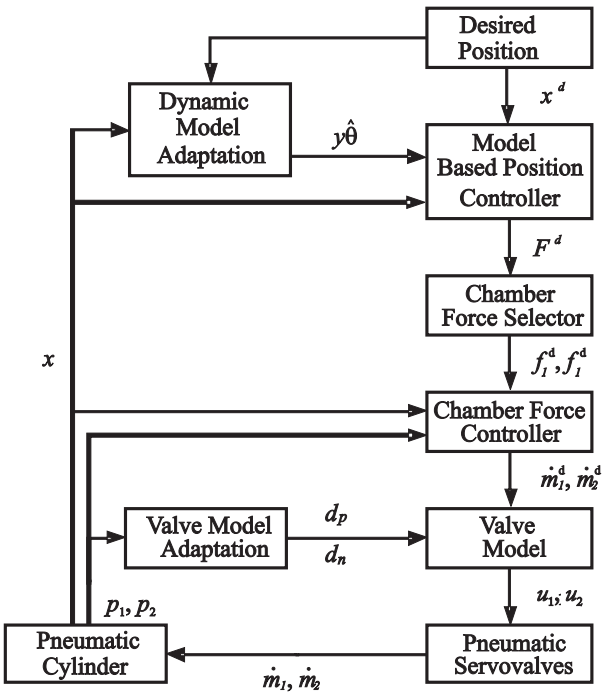

Fig. 2: *Block diagram of the adaptive pneumatic servo positioning system. The system may be used for combined position and compliance control (shown) or force control (eliminating top 3 blocks)*

The mechanical system properties (m, c, k, & η) are adapted online to approximate the unknown dynamics of the pneumatic servo system. These mechanical system properties are not meant to be the actual physical parameters, but rather serve as a basis for the unknown dynamics.

2.4 Adaptive 2nd Order System Model

The second order system parameters are grouped for the adaptive load and dynamics compensation. The terms for adaptation are mass, damping, stiffness, and external forces. These terms are grouped together using a regressor matrix, Y, and a vector of adaptive parameters, Θ, so that:

$$\mathbf{Y\Theta} = \begin{bmatrix} \dot{w} & \dot{x} & x & 1 \end{bmatrix}\begin{bmatrix} \theta_1 & \theta_2 & \theta_3 & \theta_4 \end{bmatrix}^T, \quad \text{with } \theta_1 = m,\ \theta_2 = c,\ \theta_3 = k,\ \theta_4 = \eta. \tag{7}$$

These mechanical system properties will adapt as needed to help with system tracking. By substituting Eq. 7 into Eq. 6 the model of the system becomes:

$$m\dot{s} + \mathbf{Y\Theta} = f_1 - f_2 \tag{8}$$

2.5 Adaptive Deadband Compensation Model

The spool in the valve is slightly wider than the flow channel entrance so as to reduce air leakage when the spool is at the center position. This spool overlap causes a nonlinear deadband region in the proportional valve centered between negative and positive mass flow. However, even with a large spool overlap there will be air leakage (airflow at the spool center position due to lack of a tight seal at the valve center position) that should be accounted for in the valve model. Both the deadband effect and valve leakage are included in the second part of the Lyapunov based adaptive pneumatic controller, which is described below.

Mass flow rate through a spool valve is also nonlinear with respect to pressure. As chamber pressure increases, it takes a large opening through the spool valve to achieve the same mass flow. This effect has been effectively modeled from experiments by Wolbrecht (2009) and others. However, experimental modeling is expensive and time intensive, and in many applications is not necessary because the normal operating range of the actuator is below the high pressures where the pressure nonlinearity is most severe. Furthermore, the pressure nonlinearity can be at least partially accounted for with the use of adaptation as presented here.

Regardless of chamber pressure, mass flow through the valve always increases when the valve spool position is increased. Therefore the model for mass flow rate is a piecewise combination of monotonically increasing functions of the proportional valve control signal, u . There are four separate regions as well as an offset to properly fit the valve deadband curve. The regions are separated by the adaptable positive (d_p) and negative (d_n) boundary positions. Fig. 3 below shows the piecewise spline converting the valve control signal, u, into an air mass flow rate, $\dot{m}$. The piecewise spline creates a curve fit of the proportional valve deadband using weighted monotonically increasing functions. The regions A and D are linear with a slope of 1 so that the sensitivity of mass flow rate to the valve control voltage is set by the force controller gains presented later in section 2.7.

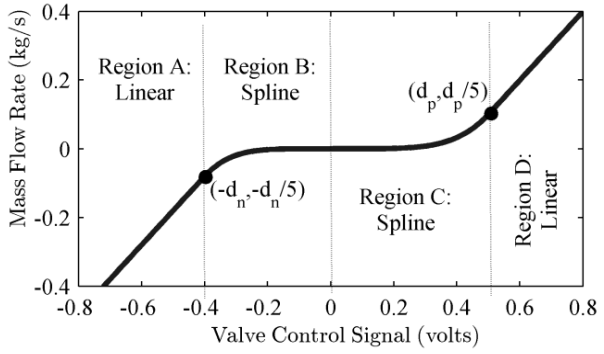

Fig. 3: *Piecewise spline modelling proportional valve deadband. This nonlinear deadband model is determined online by the adaptive controller*

The equation for regions B and C has the form

$$\dot{m}_{\text{spline}} = b_0 + b_1 u + b_2 u^5. \tag{9}$$

where b_{0-2} are adaptable coefficients. Alternative equations to Eq. 9 are possible. In particular, u^5 in Eq. 9 can be changed to any odd power (u^3, u^7, u^9 etc.). The higher the chosen power, the flatter the deadband model is around zero and the sharper the transition to the linear regions A and D. The choice may be valve specific but in most cases Eq. 9 provides reasonable deadband steepness. Additional polynomial terms could also be considered, but do not significantly change the shape of the deadband region. The equation coefficients for region C are found using the system of equations:

$$\begin{bmatrix} d_p & d_p^5 \\ 1 & 5d_p^4 \end{bmatrix} \begin{bmatrix} b_1 \\ b_2 \end{bmatrix} = \begin{bmatrix} y \\ 1 \end{bmatrix} = \boldsymbol{X} \tag{10}$$

where d_p is positive spline boundary position where the control voltage switches from the spline to the linear region, and y is the mass flow rate value at d_p. The bias b_0 is treated as a separate, additive term, as it is the same in all 4 regions. The second equation in Eq. 10 sets the spline function slope to 1 to make the first derivative of the function continuous between the spline and linear regions. The steepness of the deadband is chosen to be $y = d_p / 5$. This provides reasonable steepness while still modeling the deadband effect, and allows Eq. 10 to be solved for

$$b_1 = 0, \text{ and } b_2 = \frac{1}{5d_p^4}. \tag{11}$$

The spline function for region C is then of the form

$$\dot{m}_C = b_0 + \frac{1}{5d_p^4} u^5. \tag{12}$$

To keep the deadband model continuous, the equation for the linear region for the positive flow side (region D) is

$$\dot{m}_D = b_0 + u - \tfrac{4}{5} d_p. \tag{13}$$

By repeating the above process the mass flow equations for negative flow regions (A and B) of the deadband model may be found. All of the mass flow equations for the spline and the linear regions may be put into the general vector form

$$\dot{m} = \boldsymbol{U}\boldsymbol{B} = \boldsymbol{U}\left(\hat{\boldsymbol{B}} - \tilde{\boldsymbol{B}}\right), \tag{14}$$

where $\boldsymbol{U}$ is a regressor vector, $\boldsymbol{B}$ is the weight vector, $\hat{\boldsymbol{B}}$ is the estimate and $\tilde{\boldsymbol{B}} = \hat{\boldsymbol{B}} - \boldsymbol{B}$ is the estimate error. With this definition the mass flow equations for all four deadband model equations in Fig. 3 are defined

$$\begin{aligned}
\dot{m}_A &= \boldsymbol{U}_A \boldsymbol{B} = \left[u \quad 1 \quad +\frac{4}{5} \quad 0 \right] \boldsymbol{B} \\
\dot{m}_B &= \boldsymbol{U}_B \boldsymbol{B} = \left[0 \quad 1 \quad \frac{1}{5d_n^5} u^5 \quad 0 \right] \boldsymbol{B} \\
\dot{m}_C &= \boldsymbol{U}_C \boldsymbol{B} = \left[0 \quad 1 \quad 0 \quad \frac{1}{5d_p^5} u^5 \right] \boldsymbol{B} \\
\dot{m}_D &= \boldsymbol{U}_D \boldsymbol{B} = \left[u \quad 1 \quad 0 \quad -\frac{4}{5} \right] \boldsymbol{B} \\
\boldsymbol{B} &= \begin{bmatrix} 1 & b_0 & d_n & d_p \end{bmatrix}^T
\end{aligned} \tag{15}$$

An explicit solution for the proportional valve control signal, u, may be found for each of the mass flow equations defined in Eq. 15. This is important as the position and force controller will determine a desired mass flow rate, and deadband model equations will be used to find the necessary control signal to produce the desired flow. The resulting control signal equations as a function of desired mass flow for all four regions of the deadband model are

$$u=\begin{cases}\dot{m}^{\mathrm{d}}-b_0-\frac{4}{5}d_{\mathrm{n}} & ,\text{for } \dot{m}^{\mathrm{d}}\le -\frac{d_{\mathrm{n}}}{5}\\ \left(5d_{\mathrm{n}}^4\left(\dot{m}^{\mathrm{d}}-b_0\right)\right)^{\frac{1}{5}} & ,\text{for } -\frac{d_{\mathrm{n}}}{5}<\dot{m}^{\mathrm{d}}\le 0\\ \left(5d_{\mathrm{p}}^4\left(\dot{m}^{\mathrm{d}}-b_0\right)\right)^{\frac{1}{5}} & ,\text{for } 0<\dot{m}^{\mathrm{d}}\le \frac{d_{\mathrm{p}}}{5}\\ \dot{m}^{\mathrm{d}}-b_0+\frac{4}{5}d_{\mathrm{p}} & ,\text{for } \dot{m}^{\mathrm{d}}>\frac{d_{\mathrm{p}}}{5}\end{cases}. \tag{16}$$

2.6 Lyapunov Candidate Function

Theoretical stability may be demonstrated using Lyapunov's direct method (Spong, 1989). A passivity-based control is desired, which means the total energy of the system should be used as the candidate function. In this application, the candidate function consists of position tracking errors, force tracking errors, valve compensation parameter errors, and system gains. The candidate function is

$$\begin{aligned}V=&\tfrac{1}{2}ms^2+\tilde{x}^2\Lambda K+\tfrac{1}{2}\tilde{\boldsymbol{\Theta}}^T\boldsymbol{\Gamma}\tilde{\boldsymbol{\Theta}}+\tfrac{1}{2}\tilde{f}_1^2\Omega+\tfrac{1}{2}\tilde{f}_2^2\Omega\\&+\tfrac{1}{2}\tilde{\boldsymbol{B}}_1^T\boldsymbol{\Psi}\tilde{\boldsymbol{B}}_1+\tfrac{1}{2}\tilde{\boldsymbol{B}}_2^T\boldsymbol{\Psi}\tilde{\boldsymbol{B}}_2\end{aligned} \tag{17}$$

where m is the mass, s is the sliding surface, $\tilde{x}$ is the position error, $\tilde{\boldsymbol{\Theta}}$ is the adaptive system parameter error, $\tilde{f}_{1,2}$ are the chamber force errors, and $\tilde{\boldsymbol{B}}_{1,2}$ are errors in the valve compensation parameters. The other variables are tunable gains, either scalars (Λ, K, & Ω), or positive-definite matrices ($\boldsymbol{\Gamma}$ and $\boldsymbol{\Psi}$).

Lyapunov stability using the direct method is explained in Spong (1989). The derived negative of the candidate function derivative will be shown to be locally positive definite and therefore uniformly asymptotically stable. The derivation does not account for many of the unknown and un-modeled system dynamics and thus the proof of asymptotic stability may not hold in practice. It can however be safely assumed that the un-modeled and unknown dynamics are bounded, so at least the error from the desired signals will tend toward zero error, and stay within a region close to the desired trajectories.

The next step in proving stability is to find the derivative of the candidate function along the trajectories of the system. The derivative of Eq. 17 is:

$$\begin{aligned}\dot{V}=&sm\dot{s}+\tilde{x}\dot{\tilde{x}}2\Lambda K+\tilde{\boldsymbol{\Theta}}^T\boldsymbol{\Gamma}\dot{\tilde{\boldsymbol{\Theta}}}\\&+\tilde{f}_1\Omega\dot{\tilde{f}}_1+\tilde{f}_2\Omega\dot{\tilde{f}}_2+\tilde{\boldsymbol{B}}_1^T\boldsymbol{\Psi}\dot{\tilde{\boldsymbol{B}}}_1+\tilde{\boldsymbol{B}}_2^T\boldsymbol{\Psi}\dot{\tilde{\boldsymbol{B}}}_2\end{aligned} \tag{18}$$

By substituting the net force equation of Eq. 1, the pneumatic chamber model of Eq. 2, the system model of Eq. 8, and defining the chamber force errors as $\tilde{f}_{1,2}=f_{1,2}-f_{1,2}^{\mathrm{d}}$, Eq. 18 becomes:

$$\begin{aligned}\dot{V}=&s\left(F^{\mathrm{d}}-\mathbf{Y}\hat{\boldsymbol{\Theta}}\right)\\&+\tilde{f}_1\Omega\left(\gamma RT\frac{a_1}{v_1}\dot{m}_1-\gamma\frac{\dot{v}_1}{v_1}f_1-\dot{f}_1^{\mathrm{d}}+\frac{s}{\Omega}\right)\\&+\tilde{f}_2\Omega\left(\gamma RT\frac{a_2}{v_2}\dot{m}_2-\gamma\frac{\dot{v}_2}{v_2}f_2-\dot{f}_2^{\mathrm{d}}-\frac{s}{\Omega}\right)\\&+\tilde{x}\dot{\tilde{x}}2\Lambda K+\tilde{\boldsymbol{\Theta}}^{\mathrm{T}}\left(\boldsymbol{\Gamma}\dot{\tilde{\boldsymbol{\Theta}}}+\mathbf{Y}^{\mathrm{T}}s\right)+\tilde{\boldsymbol{B}}_1^{\mathrm{T}}\boldsymbol{\Psi}\dot{\tilde{\boldsymbol{B}}}_1+\tilde{\boldsymbol{B}}_2^{\mathrm{T}}\boldsymbol{\Psi}\dot{\tilde{\boldsymbol{B}}}_2\end{aligned} \tag{19}$$

where $\dot{f}^{\mathrm{d}}$ is the desired force derivative, and the other parameters are as described previously. Next, the mass flow model equations of Eq. 14 are substituted into Eq. 19. The Lyapunov function derivative is now:

$$\begin{aligned}\dot{V}=&s\left(F^{\mathrm{d}}-\mathbf{Y}\hat{\boldsymbol{\Theta}}\right)\\&+\tilde{f}_1\Omega\left(\gamma RT\frac{a_1}{v_1}\boldsymbol{U}_1\hat{\boldsymbol{B}}_1-\gamma\frac{\dot{v}_1}{v_1}f_1-\dot{f}_1^{\mathrm{d}}+\frac{s}{\Omega}\right)\\&+\tilde{f}_2\Omega\left(\gamma RT\frac{a_2}{v_2}\boldsymbol{U}_2\hat{\boldsymbol{B}}_2-\gamma\frac{\dot{v}_2}{v_2}f_2-\dot{f}_2^{\mathrm{d}}-\frac{s}{\Omega}\right)\\&+\tilde{x}\dot{\tilde{x}}2\Lambda K+\tilde{\boldsymbol{\Theta}}^{\mathrm{T}}\left(\boldsymbol{\Gamma}\dot{\tilde{\boldsymbol{\Theta}}}+\mathbf{Y}^{\mathrm{T}}s\right)\\&+\tilde{\boldsymbol{B}}_1^{\mathrm{T}}\left(\boldsymbol{\Psi}\dot{\tilde{\boldsymbol{B}}}_1-\Omega\gamma RT\frac{a_1}{v_1}\boldsymbol{U}_1^{\mathrm{T}}\tilde{f}_1\right)\\&+\tilde{\boldsymbol{B}}_2^{\mathrm{T}}\left(\boldsymbol{\Psi}\dot{\tilde{\boldsymbol{B}}}_2-\Omega\gamma RT\frac{a_2}{v_2}\boldsymbol{U}_2^{\mathrm{T}}\tilde{f}_2\right)\end{aligned} \tag{20}$$

2.7 Control Equations for Lyapunov Stability

The first three terms in Eq. 20 are governed by the mass flow rate through the base and rod side proportional control valves. First, the desired net cylinder force is set using the adaptive 2nd order system and negative position and velocity feedback:

$$F^{d}=\mathbf{Y}\hat{\boldsymbol{\Theta}}-Ks \tag{21}$$

The net desired force is broken down into desired rod and base side forces, using the smoothing technique developed in Wolbrecht (2009). The desired rod and base side forces are used in the mass flow equations, which are chosen to be:

$$\begin{aligned}\boldsymbol{U}_1\hat{\boldsymbol{B}}_1&=\frac{1}{\gamma RT}\frac{v_1}{a_1}\left(-\frac{g}{\Omega}\tilde{f}_1+\gamma\frac{\dot{v}_1}{v_1}f_1+\dot{f}_1^{\mathrm{d}}-\frac{s}{\Omega}\right)\\\boldsymbol{U}_2\hat{\boldsymbol{B}}_2&=\frac{1}{\gamma RT}\frac{v_2}{a_2}\left(-\frac{g}{\Omega}\tilde{f}_2+\gamma\frac{\dot{v}_2}{v_2}f_2+\dot{f}_2^{\mathrm{d}}+\frac{s}{\Omega}\right)\end{aligned} \tag{22}$$

where g is a positive gain. To simplify theses expressions, and to isolate the tunable gains, we define the following equations:

$$\begin{aligned}G_{\mathrm{f}}&=g/\Omega\gamma RT & G_{\mathrm{v}}&=1/RT\\G_{\mathrm{f^d}}&=1/\gamma RT & G_{\mathrm{s}}&=1/\Omega\gamma RT\end{aligned}. \tag{23}$$

These gain equations absorb the physical parameters (which are assumed constant) γ, R, and T. Substituting these into Eq. 22 gives:

$$\begin{aligned}\boldsymbol{U}_1\hat{\boldsymbol{B}}_1&=\frac{v_1}{a_1}\left(-G_{\mathrm{f}}\tilde{f}_1+G_{\mathrm{v}}\frac{\dot{v}_1}{v_1}f_1+G_{\mathrm{f^d}}\dot{f}_1^{\mathrm{d}}-G_{\mathrm{s}}s\right)\\\boldsymbol{U}_2\hat{\boldsymbol{B}}_2&=\frac{v_2}{a_2}\left(-G_{\mathrm{f}}\tilde{f}_2+G_{\mathrm{v}}\frac{\dot{v}_2}{v_2}f_2+G_{\mathrm{f^d}}\dot{f}_2^{\mathrm{d}}+G_{\mathrm{s}}s\right)\end{aligned} \tag{24}$$

By controlling the valve flow according to Eq. 21 and 22 the Lyapunov function derivative becomes:

$$\begin{aligned}\dot{V} = &-Ks^2 - \tilde{f}_1^2 g - \tilde{f}_2^2 g + \tilde{x}\dot{\tilde{x}} 2\Lambda K + \tilde{\boldsymbol{\Theta}}^{\mathrm{T}}\left(\boldsymbol{\Gamma}\dot{\tilde{\boldsymbol{\Theta}}} + \mathbf{Y}^{\mathrm{T}} s\right) \\ &+ \tilde{\boldsymbol{B}}_1^{\mathrm{T}}\left(\boldsymbol{\Psi}\dot{\tilde{\boldsymbol{B}}}_1 - \frac{1}{G_{\mathrm{s}}}\frac{a_1}{v_1}\boldsymbol{U}_1^{\mathrm{T}}\tilde{f}_1\right) \\ &+ \tilde{\boldsymbol{B}}_2^{\mathrm{T}}\left(\boldsymbol{\Psi}\dot{\tilde{\boldsymbol{B}}}_2 - \frac{1}{G_{\mathrm{s}}}\frac{a_2}{v_2}\boldsymbol{U}_2^{\mathrm{T}}\tilde{f}_2\right)\end{aligned} \tag{25}$$

The first term above may be expanded using the equation $s^2 = \dot{\tilde{x}}^2 + \Lambda^2\tilde{x}^2 + 2\Lambda\tilde{x}\dot{\tilde{x}}$, which simplifies Eq. 25 to:

$$\begin{aligned}\dot{V} = &-K\dot{\tilde{x}}^2 - K\Lambda^2\tilde{x}^2 - \tilde{f}_1^2 g - \tilde{f}_2^2 g + \tilde{\boldsymbol{\Theta}}^{\mathrm{T}}\left(\boldsymbol{\Gamma}\dot{\tilde{\boldsymbol{\Theta}}} + \mathbf{Y}^{\mathrm{T}} s\right) \\ &+ \tilde{\boldsymbol{B}}_1^{\mathrm{T}}\left(\boldsymbol{\Psi}\dot{\tilde{\boldsymbol{B}}}_1 - \frac{1}{G_{\mathrm{s}}}\frac{a_1}{v_1}\boldsymbol{U}_1^{\mathrm{T}}\tilde{f}_1\right) \\ &+ \tilde{\boldsymbol{B}}_2^{\mathrm{T}}\left(\boldsymbol{\Psi}\dot{\tilde{\boldsymbol{B}}}_2 - \frac{1}{G_{\mathrm{s}}}\frac{a_2}{v_2}\boldsymbol{U}_2^{\mathrm{T}}\tilde{f}_2\right)\end{aligned} \tag{26}$$

The negative of the first four terms in Eq. 26 are now clearly positive-definite.

The final three terms in the Lyapunov function candidate are made equal to zero by setting:

$$\begin{aligned}\dot{\tilde{\boldsymbol{\Theta}}} &= \dot{\hat{\boldsymbol{\Theta}}} = -\boldsymbol{\Gamma}^{-1}\mathbf{Y}^{\mathrm{T}} s = -\mathbf{G}_{\boldsymbol{\Gamma}}\mathbf{Y}^{\mathrm{T}} s \\ \dot{\tilde{\boldsymbol{B}}}_1 &= \dot{\hat{\boldsymbol{B}}}_1 = \boldsymbol{\Psi}^{-1}\frac{1}{G_{\mathrm{s}}}\frac{a_1}{v_1}\boldsymbol{U}_1^{\mathrm{T}}\tilde{f}_1 = \mathbf{G}_{\boldsymbol{\Psi}}\frac{a_1}{v_1}\boldsymbol{U}_1^{\mathrm{T}}\tilde{f}_1 \\ \dot{\tilde{\boldsymbol{B}}}_2 &= \dot{\hat{\boldsymbol{B}}}_2 = \boldsymbol{\Psi}^{-1}\frac{1}{G_{\mathrm{s}}}\frac{a_2}{v_2}\boldsymbol{U}_2^{\mathrm{T}}\tilde{f}_2 = \mathbf{G}_{\boldsymbol{\Psi}}\frac{a_2}{v_2}\boldsymbol{U}_2^{\mathrm{T}}\tilde{f}_2\end{aligned} \tag{27}$$

where $\mathbf{G}_{\boldsymbol{\Gamma}}$ and $\mathbf{G}_{\boldsymbol{\Psi}}$ are gain matrices. The above are known as the parameter update equations, and govern how the controller changes the parameters in order to improve tracking performance. By substituting Eq. 27 into Eq. 26, the final expression of the candidate function is

$$\dot{V} = -K\dot{\tilde{x}}^2 - K\Lambda^2\tilde{x}^2 - \tilde{f}_1^2 g - \tilde{f}_2^2 g\,, \tag{28}$$

which makes $-\dot{V}$ positive definite and theoretically proves asymptotic stability of the controller. In practice, however, the presence of un-modeled system dynamics such as pressure waves, sensor dynamics, analog-to-digital conversion (ADC), and digital-to-analog conversion (DAC), limits the stable magnitudes of system gains.

Because of the piecewise nature of the deadband compensation model, the parameter update laws for $\dot{\hat{\boldsymbol{B}}}_1$ and $\dot{\hat{\boldsymbol{B}}}_2$ are different depending on which of the four regions of the deadband model the system currently resides. Combining Eq. 15 and 27, the base side deadband parameter update laws are:

$$\begin{aligned}\dot{\hat{\boldsymbol{B}}}_{1,\mathrm{A}} &= \mathbf{G}_{\boldsymbol{\Psi}}\frac{a_1}{v_1}\begin{bmatrix} u_1 & 1 & +\frac{4}{5} & 0\end{bmatrix}^{\mathrm{T}}\tilde{f}_1 \\ \dot{\hat{\boldsymbol{B}}}_{1,\mathrm{B}} &= \mathbf{G}_{\boldsymbol{\Psi}}\frac{a_1}{v_1}\begin{bmatrix} 0 & 1 & \frac{1}{5d_{\mathrm{n}}^5}u_1^5 & 0\end{bmatrix}^{\mathrm{T}}\tilde{f}_1 \\ \dot{\hat{\boldsymbol{B}}}_{1,\mathrm{C}} &= \mathbf{G}_{\boldsymbol{\Psi}}\frac{a_1}{v_1}\begin{bmatrix} 0 & 1 & 0 & \frac{1}{5d_{\mathrm{p}}^5}u_1^5\end{bmatrix}^{\mathrm{T}}\tilde{f}_1 \\ \dot{\hat{\boldsymbol{B}}}_{1,\mathrm{D}} &= \mathbf{G}_{\boldsymbol{\Psi}}\frac{a_1}{v_1}\begin{bmatrix} u_1 & 1 & 0 & -\frac{4}{5}\end{bmatrix}^{\mathrm{T}}\tilde{f}_1 \\ \boldsymbol{B}_1 &= \begin{bmatrix}1 & b_{0,1} & d_{\mathrm{n},1} & d_{\mathrm{p},1}\end{bmatrix}^{\mathrm{T}}.\end{aligned} \tag{29}$$

The appropriate parameter update law is used depending upon which region the desired flow lies with respect to Fig. 3. A similar set of parameter update laws are used for the rod side parameters which are defined as

$$\boldsymbol{B}_2 = \begin{bmatrix}1 & b_{0,2} & d_{\mathrm{n},2} & d_{\mathrm{p},2}\end{bmatrix}^{\mathrm{T}}. \tag{30}$$

Controller Tuning Procedure

A systematic procedure for tuning the system gains can greatly reduce the time and effort spent optimizing the system performance. For all tunings, a minimum chamber force, f_0, for both base and rod side force equations is set above the atmospheric force to guarantee positive flow potential into and out of the cylinder chambers. This minimum force effectively sets the compliance of the actuator and may be changed as required by the application. The controller gains, along with their tuned values used for testing, are given in order of tuning below:

$$\begin{aligned} G_{\mathrm{f}} &= 0.012 \qquad K = 0.04 \\ G_{\mathrm{v}} &= 0.00002 \qquad \Lambda = 300 \\ G_{\mathrm{f^d}} &= 0.0005 \quad G_s = 0.0007 \\ \mathbf{G}_{\boldsymbol{\Psi}} &= \begin{bmatrix} 0 & 0 & 0 & 0 \\ 0 & 0.3 & 0 & 0 \\ 0 & 0 & 0.05 & 0 \\ 0 & 0 & 0 & 0.05 \end{bmatrix} \\ \mathbf{G}_{\boldsymbol{\Gamma}} &= \begin{bmatrix} 0.001 & 0 & 0 & 0 \\ 0 & 0.001 & 0 & 0 \\ 0 & 0 & 0.06 & 0 \\ 0 & 0 & 0 & 0.1 \end{bmatrix} \end{aligned} \tag{31}$$

The tuning procedure begins with force control and with the desired net force set to zero. Tuning is performed while the rod is manually moved in and out. The force error gain, G_{f}, is gradually increased from zero until ease of movement is achieved but before chattering occurs. The next gain adjusts a positive feedback term that provides mass flow in order to keep up with the changing cylinder volumes. This gain is defined by $G_{\mathrm{v}} = 1 / RT$, so tuning this gain effectively defines the mean operating temperature, although its value is chosen based on system performance. This chamber velocity linearization gain is gradually increased to the point where the positive feedback is apparent. This occurs when pushing the cylinder in one direction elicits a noticeable push in the same direction from the controller. The value is then reduced by approximately 20 %.

The desired force derivative gain, $G_{\mathrm{f^d}}$, is a feed forward acceleration based gain that helps reducing the phase lag between the desired and actual force. This gain is theoretically related to G_{v} where $G_{\mathrm{v}}/G_{\mathrm{f^d}} = \gamma = 1.4$. In practice, however, the presence of system noise and un-modeled dynamics limits the magnitude of G_{f^d} and proper tuning typically leads to a lower value. Tuning $G_{\mathrm{f^d}}$ requires force tracking. If main operational frequency is known, then the gain can be tuned to that base frequency. Otherwise a range of about 0.5 - 3 Hz should be used to tune the gain to the phase. The phase lag may not be eliminated completely

so the desired force derivative gain should not be set too high, as this may cause instability for other desired force trajectories

The next step is to tune the position tracking which requires adjusting multiple gains. The desired net force gain, K, and the sliding surface gain, Λ, are essentially proportional-derivative gains for position tracking. These gains produce a desired net force depending on the desired position and velocity errors. Once K and Λ are tuned, the sliding surface gain, G_s, may be adjusted. The sliding surface gain bypasses the desired force and directly contributes to the desired mass flow based on position and velocity tracking errors. This gain is multiplied by the sliding surface which contains the gain, Λ, making the tuning of the three position tracking gains in this paragraph interdependent.

The next steps tune the adaptive parameters of the system that help with all tracking and varying load conditions, and therefore should not be over-tuned to a specific set of conditions. The adaptive valve compensation gain, $\boldsymbol{G}_\psi$, is first to tune. This matrix gain includes three nonzero scalars on the diagonal. The first scalar is the adaptation rate of the leakage estimation parameter, b_0, and the second two other scalars are the adaptation rate for the spline transition points d_n and d_p, as previously defined. All three of these gains are increased slowly from zero during force tracking while watching both the tracking performance and adaptation rates. The tuning goal is to optimize tracking while keeping adaptation rates at a minimum. Once good performance is achieved at the desired force tracking frequencies, the adaptive valve compensation parameters are fixed for position tracking. This process successfully identifies the deadband of the valve and may be repeated periodically to re-calibrate the deadband model and re-optimize force tracking performance.

The final gain to tune is the adaptive system gain, $\boldsymbol{G}_\Gamma$. This matrix gain includes four nonzero scalars on the diagonal that allow the controller to improve performance by adaptively estimating mass, viscous friction, spring constant, and external force terms. As these values are not expected to change rapidly, the adaptation rates should be minimized while allowing adequate performance.

It is important during the tuning process to test a dynamically diverse set of desired trajectories, such as sine, square, and sawtooth waveforms at different frequencies. Also, perturbations and external forces (pushing and pulling and varying load weights) on the rod should be explored. This will identify instabilities and help ensure a stable controller for a wide range of applications.

3 Experimental Hardware

An experimental system was used to test the adaptive pneumatic controller. The linear actuator is a Bimba PFC-092-XBL low-friction, double-acting pneumatic cylinder. Integrated in the cylinder is a linear motion potentiometer (LMP) for measuring the stroke position. The cylinder has a 51 mm stroke with a 27 mm bore. The linearity is ± 1 percent of the stroke, and the mechanical repeatability is ± 0.025 mm. The LMP is supplied 5 volts direct current (VDC) for the experiments.

Two Honeywell ASCX100AN pressure sensors measure pressure independently in both the base and rod cylinder chambers. Each sensor measures absolute pressure from 0 - 690 kPa. The 100 µS response time of the pressure sensor is acceptable for the 1 kHz controller sampling and control frequency. For the laboratory experiments the supply pressure was approximately 620 kPa.

Two proportional Festo MPYE-5-1/8-HF-010-B pneumatic valves are used to control flow in and out of each cylinder chamber. The internal valve driver provides closed loop control of the spool position. According to the manufacturer, the valve has a nominal flow rate of 700 L/min and a 100 Hz bandwidth.

The adaptive pneumatic controller was implemented using Simulink® and xPC Target for hardware-in-the-loop (HIL) testing. Data acquisition and control for the experiment is implemented using Measurement Computing DAS1200 PCI computer card on the target computer. The data acquisition card has 8 differential 12-bit analog-to-digital converter channels with a 330 kS/s sample rate and two 12-bit digital-to-analog channels used for controlling the proportional valves.

A passive analog RC anti-aliasing filter was used on the pressure and position signals. The filter had 284 Hz low-pass Butterworth cut-off frequency. The velocity used for the controller was approximated from a discrete derivate of the position signal passed through a discrete 100 Hz low-pass Butterworth filter. This velocity filtering corner frequency is well above the expected cylinder operating frequency of 0 to 5 Hz.

4 Testing and Results

The pneumatic servo system is tested using force and position control of several repetitive waveforms to show the tracking accuracy. The first set of tests uses force control to learn the deadband compensation model. The deadband parameters are then fixed during force and position control testing. The second set of tests shows the force control for three different waveforms: sine, square, and sawtooth. The third set of tests shows the adaptive system dynamics compensation. The fourth set of tests shows position control for three different waveforms: sine, square, and sawtooth. Finally, the last section will show the servo system position tracking with external disturbances like impacts and constant offset forces. The results show marked improvements when adaptation is used and the ability to accurately track force and position with load variations.

4.1 Adaptive Deadband Compensation Testing

The deadband model boundary positions are tested for convergence during force control of a sinusoidal waveform from 1 - 5 Hz. The desired force has a 135 N peak-to-peak swing with a 135 N offset force on top of

the 110 N minimum force. This desired force trajectory spans a majority of the operating range of the pneumatic cylinder for a supply pressure of approximately 6 bar.

The adaptation of the base side deadband spline boundary parameters is shown below in Fig. 4.

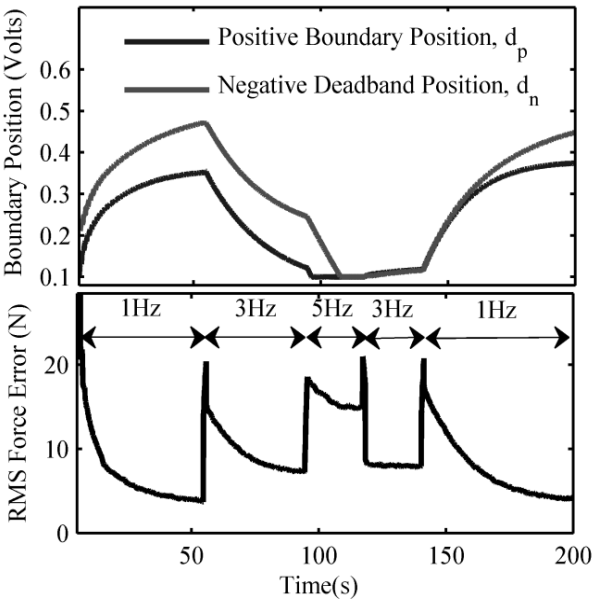

Fig. 4: *Adaptation of the base side valve deadband model during force tracking of changing input frequencies*

As the deadband model adapts the root-mean-squared (RMS) force error falls exponentially while the valve boundary positions converge to similar values for similar frequencies. This is true for the initial 1 Hz desired and the return to 1 Hz desired force at the end of the test. Results from the rod side were similar, although the resulting boundary positions are larger than the base side positions. The rod side also converges more quickly than the base side. This is due to the smaller volume of the rod side chamber because of the presence of the piston rod.

The deadband compensation model is intended to map the proportional valve voltage to actual mass flow. Because this deadband compensation is steady-state, it is appropriate to choose boundary values that have adapted to relatively low desired force frequencies. For this reason, the converged deadband boundary lengths from 1 Hz force tracking experiment were selected and then fixed for the position tracking tests. The resulting values for both base and rod sides, in terms of proportional valve control voltage, are:

$$\begin{aligned} d_{\text{n,base}} &= 0.515, \quad d_{\text{p,base}} = 0.354 \\ d_{\text{n,rod}} &= 0.389, \quad d_{\text{p,rod}} = 0.549 \end{aligned} \tag{32}$$

4.2 Force Control Testing

This section describes force tracking results at various frequencies for sinusoidal, square, and sawtooth waveforms. The three repetitive waveforms give a good coverage of smooth, quick jump, and linear tracking movements. For the sake of brevity, results for only the base side chamber of the actuator will be shown. The results for the rod side chamber are similar with only slight differences occurring due to the smaller chamber volume. In all cases the cylinder was held at mid-stroke.

The results of force tracking for the base side pneumatic chamber are shown below for a desired 1 Hz (Fig. 5), 3 Hz (Fig. 6), and 5 Hz (Fig. 7) sinusoidal wave.

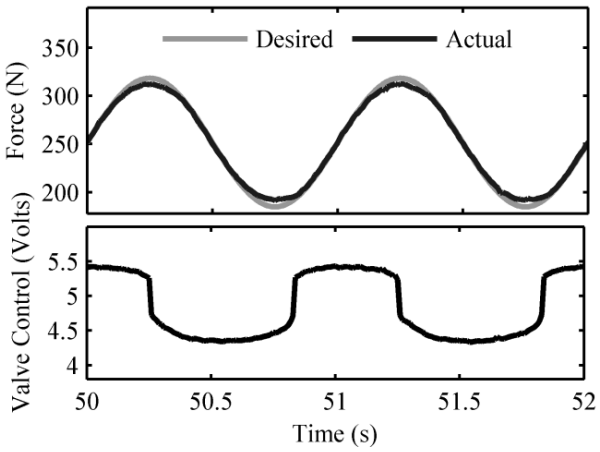

Fig. 5: *Base side force tracking at 1 Hz*

The results in the 3 figures show accurate phase for the 1 Hz tracking. The tracking degrades as expected as the frequency increases from 1 to 5 Hz. The proportional valve control signals show an appropriate swift jump across the valve deadband region (valve midpoint at 5 Volts) due to the deadband compensation model.

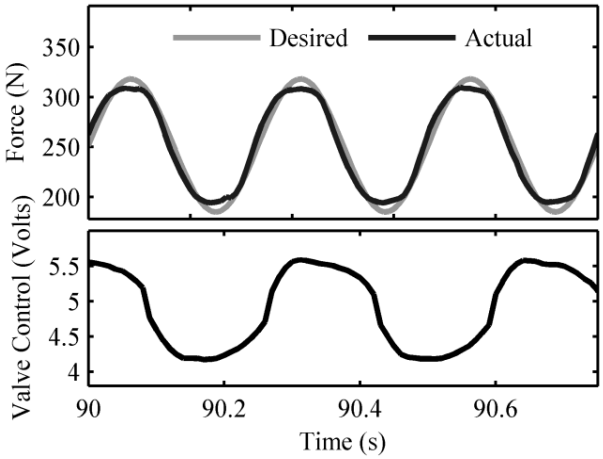

Fig. 6: *Base side force tracking at 3 Hz*

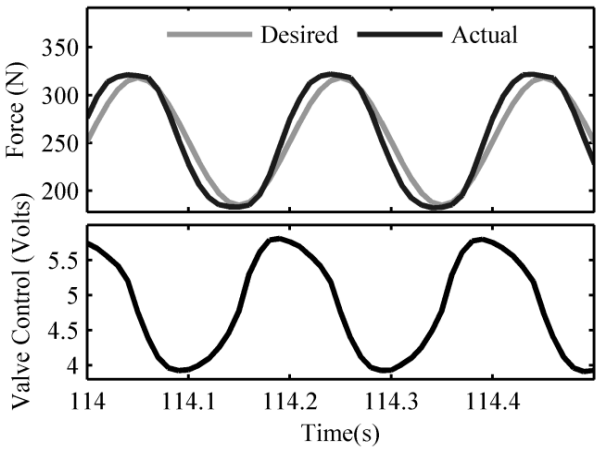

Fig. 7: *Base side force tracking at 5 Hz*

The next set of tests show force tracking of a 1 Hz sawtooth wave (Fig. 8) and a 1 Hz square wave (Fig. ***9***). Tracking a sawtooth or square introduces a discontinuity in the desired force and therefore cannot be perfectly tracked even under ideal conditions. The results, however, can provide a good evaluation of the controller performance. As seen in Fig. 8 below, although the sawtooth force tracking does not reach the peaks, there is no overshoot or oscillations after the step jump. The linear tracking region stays close to the desired signal with minimal perturbations. The square wave shows both positive and negative force step changes. The square wave shows explicitly that the settling time for exhausting is longer than that for sourcing. As the square and sawtooth force tracking increases in frequency an overshoot develops at quick force jumps.

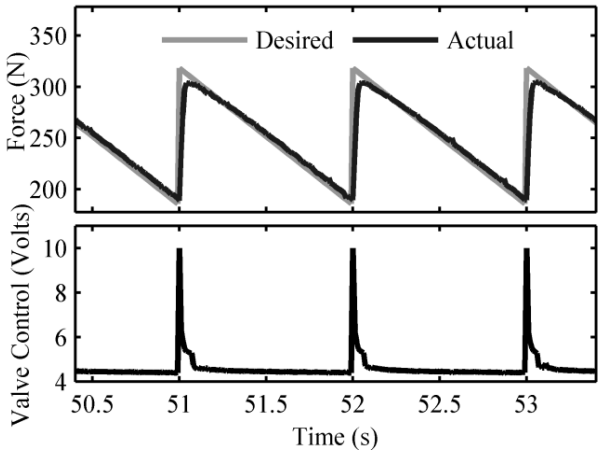

Fig. 8: *Base side force tracking of a sawtooth wave*

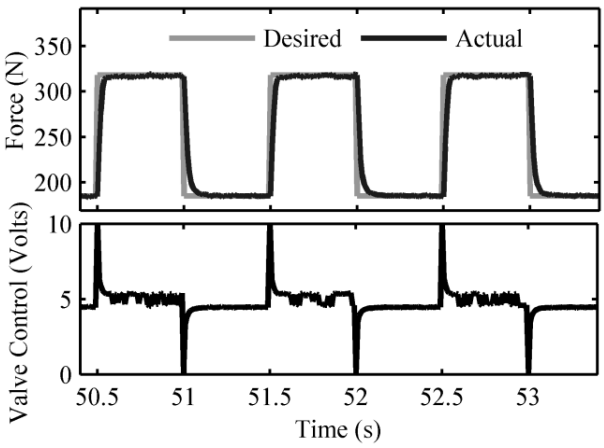

Fig. 9: *Base side force tracking of a square wave*

4.3 Position Tracking Testing

The adaptive 2nd order system helps to compensate for varying loading and environmental conditions. Position control using a 1 Hz sinusoidal wave with a 3.8 cm magnitude is used to show the effects of the adaptive system. For position tracking the deadband boundary positions are fixed, but the leakage compensation is still adapting. The minimum force was set to 110 N, and the deadband boundary positions were fixed to the values given in Eq. 32 and the tuned system gain values are given in Eq. 31. The leakage estimation parameter, b_0, is allowed to change during force and position control.

The first test of the controller without the adaptive system is shown below in Fig. 10. Note that the system was not over-tuned for position tracking. This gives the adaptive system the flexibility to compensate for a wider load and system dynamics range. The position tracking result in Fig. 10 shows a clear phase lag and amplitude error. The chamber forces in the bottom plot also show poor tracking performance.

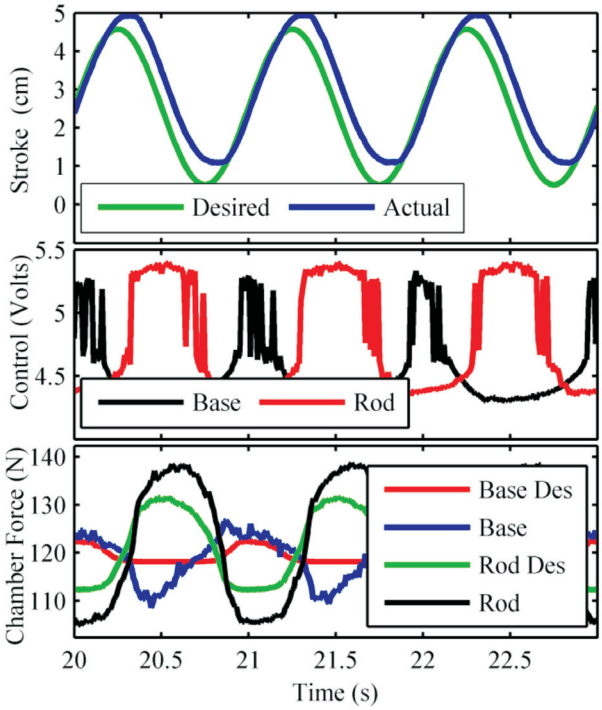

Fig. 10: *Position tracking at 1 Hz without 2nd order system adaptation*

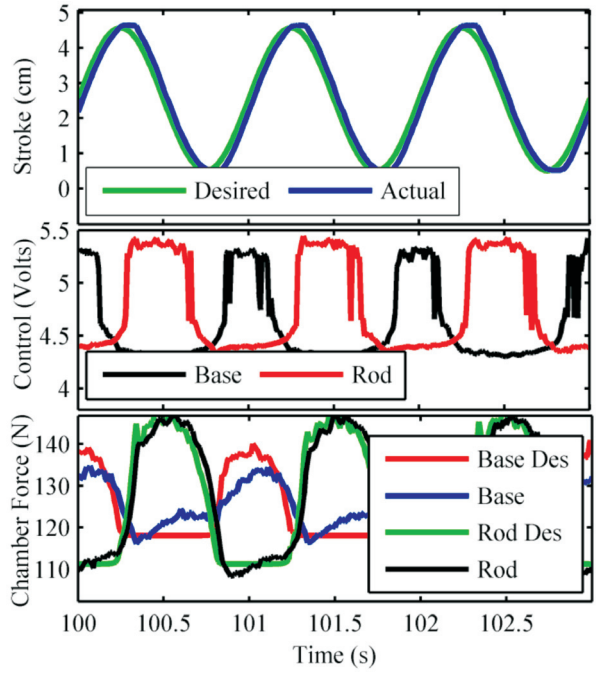

Fig. 11: *Position tracking with 1 Hz 2nd order system adaptation with the rod unloaded*

The second test for the adaptive system is done using the adaptive system with no load on the rod as shown in Fig. 11. Compared to Fig. 10, the position and force tracking are much closer than without the 2nd order system adaptation. In addition, the force tracking for both base and rod side air chambers is clearly superior to the un-adaptive controller.

The second test for the adaptive system is done using the adaptive system with no load on the rod as shown in Fig. 11. Compared to Fig. 10, the position and force tracking are much closer than without the 2nd order system adaptation. In addition, the force tracking for both base and rod side air chambers is clearly superior to the un-adaptive controller.

The next test for the adaptive system is done with a weight (17 N) attached to the rod with the cylinder in the vertical position. The results are shown in Fig. 12 below. The additional mass reduces the natural frequency of the system, but increases nonlinear friction. The steady-state tracking is similar than that without a load, which demonstrates the ability of the controller to adapt to changing mechanical parameters. The rod side chamber forces are larger than the previous experiments, as expected in order to move the larger weight against gravity.

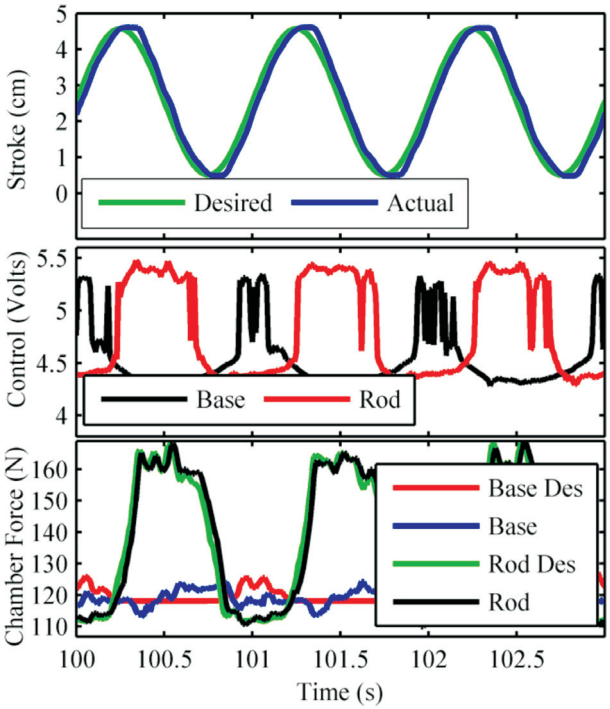

Fig. 12: *Position tracking at 1 Hz with 2nd order system adaptation with the rod loaded with a 16.9 N weight*

The position tracking performance was also tested at a frequency of 5 Hz as shown in Fig. 13 below. In these tests the magnitude of the desired sine wave was kept at 3.8 cm. As the sinusoidal frequency is increased, the position and force tracking degrades as expected. The position phase lag increases at higher frequencies as expected.

A final set of position tracking experiments used sawtooth and square waveforms. The tracking performance of a 1 Hz sawtooth (Fig. 14) and a 1 Hz square wave (Fig. 15) are shown below. The response of the controller system to quick jumps in both waveforms is limited due to the system dynamics of the proportional valve and pneumatic actuator. This creates the lag from abrupt position jumps.

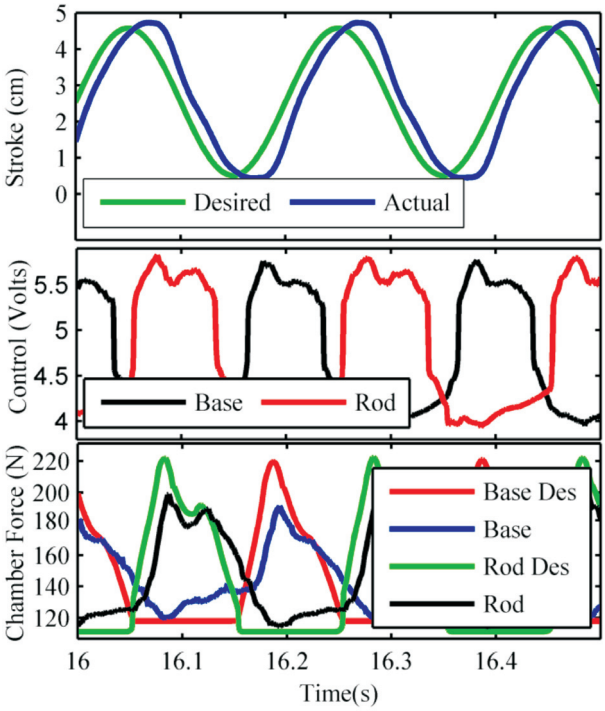

Fig. 13: *Position tracking at 5 Hz with 2nd order system adaptation*

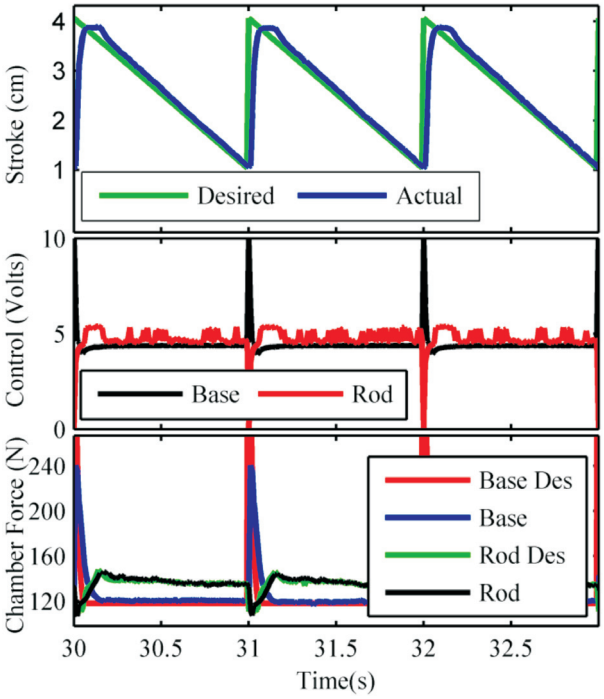

Fig. 14: *Position tracking of a 1 Hz sawtooth wave with 2nd order system adaptation*

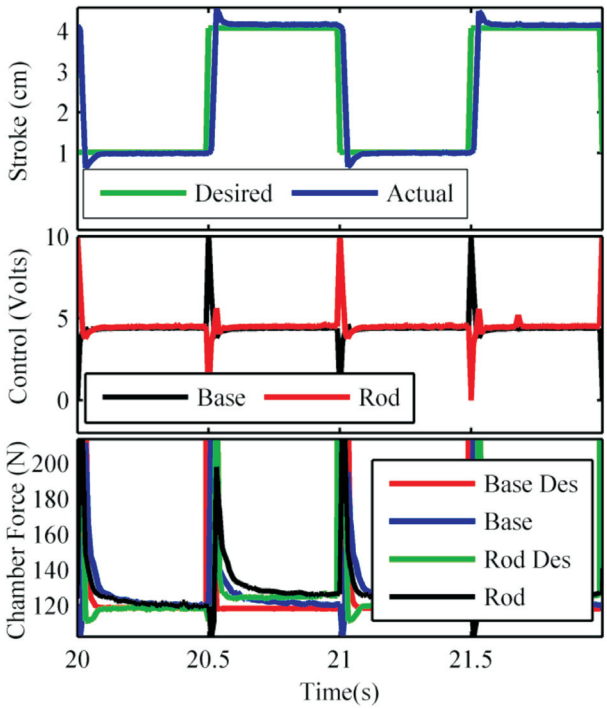

Fig. 15: *Position tracking of a 1 Hz square wave with 2nd order system adaptation*

4.4 Position Tracking with Disturbances

The adaptive pneumatic controller was also tested with external forces applied to the rod to show the stability of the system. Two tests were performed; the first added external impacts to the rod during position tracking of a 1 Hz sine wave (Fig. 16) and the second included a sudden change in external load (Fig. 17).

In Fig. 16 the impacts are evident when the position tracking suddenly deviates sharply from the desired trajectory. Although there is some overshoot in the response from the controller, it is clear that the controller is able to quickly reduce tracking error back to the previous levels. In addition, none of the impacts experimentally tested caused any instability.

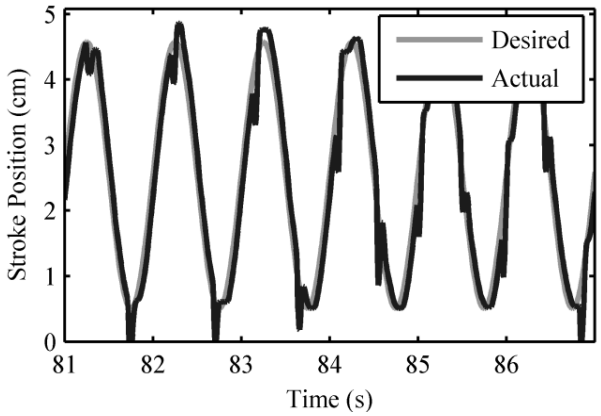

Fig. 16: *Position tracking of a 1 Hz signal with external impacts*

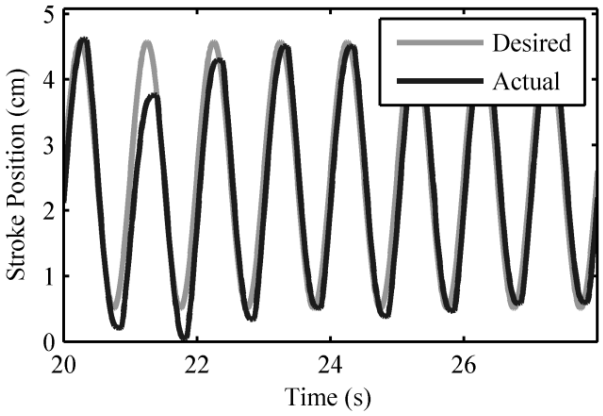

Fig. 17: *Position tracking of a 1 Hz signal with a step change in external load*

When the constant external force was suddenly applied in Fig. 17 the error in position is evident in the second peak which is approximately 60 % of the desired magnitude. The 2nd order system adaptation of the controller is able to bring the tracking error back to acceptable pre-load levels within 3 periods of the desired position signal.

5 Conclusions

This paper described an adaptive pneumatic controller for a pneumatic servo system that includes a novel deadband compensation model. The controller was shown to be theoretically stable using Lyapunov's direct method. Through experimental testing, the deadband model successfully identified the deadband characteristics of a spool type proportional pneumatic valve. Once the deadband was properly identified, it was experimentally shown to improve both force and position tracking for a variety of desired waveforms.

In practice, deadband compensation and system adaptation are a critical part of pneumatic servo control systems. This is because the nonlinear characteristics are unique to each proportional valve and each pneumatic servo system in general. Without deadband compensation, the tendency in pneumatic control systems is to over-tune the feedback gains which can lead to chattering and instability.

Future work is necessary to develop a more concise gain tuning procedure. One possible solution may be to use a separate gain optimization routine to identify the controller gains. In particular, it would be advantageous to determine gains automatically when the desired controller performance changes. For example, in some applications force control is the most important criteria, whereas other applications require precise position control.

Nomenclature

γ	ratio of specific heats for air	
$\boldsymbol{\Gamma}$	adaptive system term gain	
η	adaptive system equivalent external forces	[N]
$\boldsymbol{\Theta}$	adaptive system parameters	
Λ	sliding surface gain	[1/s]
$\boldsymbol{\Psi}$	valve compensation adaptation rate	
Ω	force error term gain	[m/(N·s)]
$a_{1,2}$	chamber area, base and rod	[m^2]
$\boldsymbol{B}$	adaptive valve parameter vector	
b_0	deadband spline offset coefficient	[kg/s]
b_1	deadband spline coefficient	[kg/(s·V)]
b_2	deadband spline coefficient	[kg/(s·V^5)]
c	adaptive system equivalent damping term	[N·s/m]
d_p	valve spline deadband control voltage position positive boundary position	[V]
d_n	valve spline deadband control voltage position negative boundary position	[V]
$f_{1,2}$	chamber force, base and rod	[N]
f_{atm}	force due to atmospheric pressure on cylinder rod	[N]
F	net cylinder force	[N]
g	Lyapunov function force error coefficient	[m/(N·s)]
G_f	desired force gain	[s/m^2]
G_{f^d}	desired force derivative gain	[s^2/m^2]
G_s	sliding surface term gain	[kg/m^2]
G_v	velocity term gain	[s^2/m^2]
$\mathbf{G}_\Gamma$	adaptive system adaptation rates	
$\mathbf{G}_\Psi$	adaptive valve spline adaptation rates	
k	external load stiffness	[N/m]
K	desired total force sliding surface gain	[N·s/m]
m	adaptive system equivalent mass term	[kg]
$\dot{m}_{1,2}$	mass flow rate, base and rod	[kg/s]
$p_{1,2}$	chamber pressure, base and rod	[Pa]
p_A	atmospheric pressure	[Pa]
p_s	supply pressure	[Pa]
R	specific gas constant for air	[J/(kg·K)]
s	sliding surface	[m/s]
T	temperature	[K]
$\boldsymbol{U}$	adaptive valve variable vector	
$u_{1,2}$	valve control signal, base and rod	[V]
v	cylinder chamber volume	[m^3]
V	lyapunov candidate function	
w	reference trajectory	[m/s]
x	rod stroke position	[m]
x^d	desired rod stroke position	[m]
y	spline boundary for mass flow	[kg/s]
$\mathbf{Y}$	adaptive system regressor matrix	

References

Bobrow, J. E. and **Jabbari, F.** 1989. Adaptive pneumatic force actuation and position control. *American Control Conference*, Pittsburgh, PA.

Bobrow, J. E. and **Lum, K.** 1996. Adaptive, high bandwidth control of a hydraulic actuator. *Journal of Dynamic Systems, Measurement, and Control*. Vol. 118. pp. 714 - 721.

Bobrow, J. E. and **McDonell, B. W.** 1998. Modeling, identification, and control of a pneumatically actuated, force controllable robot. *IEEE Transactions on Robotics and Automation*. Vol. 14. pp. 732 - 742.

Bone, G. M. and **Ning, S.** 2007. Experimental comparison of position tracking control algorithms for pneumatic cylinder actuators. *IEEE/ASME Transactions on Mechatronics*. Vol. 12. pp. 557 - 561.

Gross, D. C., **Rattan, K. S.,** 1998. An adaptive multilayer neural network for trajectory trackingcontrol of a pneumatic cylinder. *IEEE International Conference on Systems, Man, and Cybernetics*, San Diego, CA.

Knohl, T. and **Unbehauen, H.** 2000. Adaptive position control of electrohydraulic servo systems using ANN. *Mechatronics*. Vol. 10. pp. 127 - 143.

Kosaki, T. and **Sano, M.** 1997. Adaptive gain control of pneumatic servo systems with disturbance observers and fuzzy logic. *23rd International Conference on Industrial Electronics, Control and Instrumentation (IECON)*, New Orleans, LA.

McCloy, D. and **Martin, H. R.** 1980. *Control of fluid power: Analysis and design.* Ellis Horwood.

Recker, D., **Kokotovic, P.,** 1991. Adaptive nonlinear control of systems containing a deadzone. *Proceedings of the 30th IEEE Conference on Decision and Control*, Brighton, UK.

Renn, J. C. 2002. Position control of a pneumatic servo cylinder using fuzzy-sliding surface controller. *International Journal of Fluid Power*. Vol. 3. pp. 19 - 25.

Richer, E. and **Hurmuzlu, Y.** 2000. A high performance pneumatic force actuator system: Part I-Nonlinear mathematical model. *Journal of Dynamic Systems, Measurement, and Control*. Vol. 122. pp. 416 - 425.

Selmic, R. R. and **Lewis, F. L.** 2000. Deadzone compensation in motion control systems using neural networks. *IEEE Transactions on Automatic Control*. Vol. 45. pp. 602 - 613.

Shen, X. and **Goldfarb, M.** 2007. Simultaneous force and stiffness control of a pneumatic actuator. *Journal of Dynamic Systems, Measurement, and Control*. Vol. 129. pp. 425 - 434.

Slotine, J. J. E. and **Li, W.** 1987. On the adaptive control of robot manipulators. *The International Journal of Robotics Research*. Vol. 6. pp. 49 - 59.

Smaoui, M., **Brun, X.,** 2008. High-order sliding mode for an electropneumatic system: A robust differentiator-controller design. *International Journal of Robust and Nonlinear Control*. Vol. 18. pp. 481 - 501.

Spong, M. W. and **Vidyasagar, M.** 1989. *Robot dynamics and control*. Wiley.

Tao, G. and **Kokotovi, P.** 1995. Discrete-time adaptive control of systems with unknown deadzones. *International Journal of Control*. Vol. 61. pp. 1 - 17.

Valdiero, A. C. and **Bavaresco, D.,** 2008. Experimental identification of the dead zone in proportional directional pneumatic valves. *International Journal of Fluid Power*. Vol. 9. pp. 27 - 33.

Valdiero, A. C. and **Guenther, R.,** 2005. New methodology for identification of the dead zone in proportional directional hydraulic valves. *18th International Congress in Mechanical Engineering*, Ouro Preto, MG.

Wolbrecht, E. T. and **Reinkensmeyer, D. J.,** 2009. Pneumatic control of robots for rehabilitation. *The International Journal of Robotics Research*. Vol. 29. pp. 23 - 28.

Xiang, F. and **Wikander, J.** 2004. Block-oriented approximate feedback linearization for control of pneumatic actuator system. *Control Engineering Practice*. Vol. 12. pp. 387 - 399.

Eric Wolbrecht
received the B.S. degree in mechanical engineering from Valparaiso University, Valparaiso, IN, in 1996, the M.S. degree in mechanical engineering from Oregon State University, Corvallis, in 1998, and the Ph.D. degree in mechanical and aerospace engineering from the University of California, Irvine, in 2007. He is currently an Assistant Professor in the Department of Mechanical Engineering at the University of Idaho. His research interests include robotics, state estimation, nonlinear and adaptive control, pneumatic control, compliant actuation, motor learning, and neuro-rehabilitation. Dr. Wolbrecht is a member of the American Society of Mechanical Engineering and the Institute of Electrical and Electronics Engineers.

Lucas Wells
Born on August 7, 1985 in Twin Falls, ID (USA). He received his BS and MS in Electrical Engineering from the University of Idaho where he worked on pneumatic control systems and microelectronic power converters.